Investigation of delamination mechanisms during a laser drilling on a cobalt-base superalloy

Jérémy Girardot, Matthieu Schneider, Laurent Berthe, Véronique Favier

Investigation of delamination mechanisms during a laser drilling on a cobalt-base superalloy☆

J. Girardot*, M. Schneider, L. Berthe, V. Favier

Arts et Metiers ParisTech, PIMM UMR CNRS 8006, 151 Bd de l'Hôpital, 75013 Paris, France

Keywords:
Cobalt-base superalloy
Laser drilling
Fast camera analysis
Thermal barrier coating
Haynes 188

A B S T R A C T

Temperatures in the high pressure chamber of aircraft engines are continuously increasing to improve the engine efficiency. As a result, constitutive materials such as cobalt and nickel-base superalloys need to be thermally protected. The first protection is a ceramic thermal barrier coating (TBC) cast on all the hot gas-exposed structure. The second protection is provided by a cool air layer realized by the use of a thousand of drills on the parts where a cool air is flowing through. The laser drilling process is used to realize these holes at acute angles. It has been shown on coated single crystal nickel-base superalloy that the laser drilling process causes an interfacial cracking (also called delamination), detected by a cross section observation. The present work aims at characterizing interfacial cracking induced by laser drilling on coated cobalt-base super alloy. On the one hand, this work attempted to quantify the crack by several microscopic observations with regards to the most significant process parameters related as the angle beam. On the other hand, we studied the difference of the laser/ceramic and the laser/substrate interaction with real time observation by using a fast movie camera.

1. Introduction

In order to reduce gases emission and improve engine efficiency, temperatures in the high pressure chamber of aircraft engines are continuously increasing (currently up to 2300 K). As a result, constitutive materials such as cobalt and nickel-base superalloys need to be thermally protected. The first protection consists in covering the hot gas-exposed structure with a ceramic thermal barrier coating (TBC) and a bond coating (BC) (Fig. 1). The second protection is provided by a cool air layer produced by the use of thousands of drills made on the components through which a cool air is flowing. This protection method is illustrated in Fig. 2 where the typical geometry of a turbine blade in an aircraft high pressure chamber is shown.

Laser drilling is a non-contact machining process which is very useful to make acute angled holes. Two different drilling modes, labeled as percussion drilling and trepan drilling are typically used in the industry. The percussion mode is a fixed beam drilling whereas the trepan mode involves cutting with a circular trajectory centered with the hole. The range of power density generally used for both trajectories is about 1–50 MW/cm^2 during a pulse of about 1 ms. In percussion drilling mode, multiples pulses are produced until the breakthrough of the sheet. The advantage of this last method with regard to the trepan mode is a reduction in processing time by a factor of four (Sezer et al., 2006). In this range of power density, the physics process consists in heating the surface by focusing the laser beam with temperatures up to the vapor point. The melt part is then ejected by the vapor pressure and the hole is created (Semak, 1997). In this study, only the percussion mode was used to drill.

Laser drilling induces different types of defects such as a recast layer and spatters on the surface (Sezer et al., 2006) which are already observed in literature by means of cross section observation. Especially, the effect of the process parameters on the different heat affected layer across the hole was studied. Voisey et al. (2004) studied the effect of assist gas pressure on the geometry and the residual metallurgical state after a percussion laser drilling. It has been reported that the pressure and the nature of the gas have no mechanical or chemical effect on the component. On the contrary, the angle beam, its power density and the repetition rate are three parameters which modify the geometry of the hole and the size of the recast layer.

But as report in Sezer et al. (2006) and Sezer and Li (2009), the major default is the delamination of TBC. Delamination is cracking which leads to failure of the coating, damaging the turbine engine.

* Corresponding author. Tel.: +33 1 71 93 65 62.
E-mail addresses: jeremie.girardot@ensam.eu (J. Girardot), matthieu.schneider@ensam.eu (M. Schneider), laurent.berthe@ensam.eu (L. Berthe), veronique.favier@ensam.eu (V. Favier).

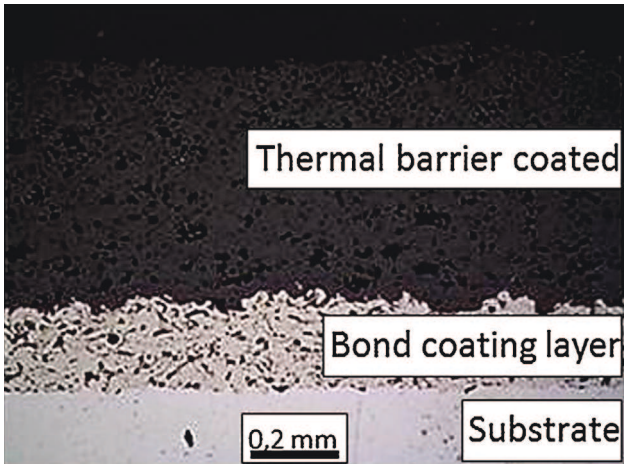

Fig. 1. Micrography of the multilayer material used in critical aircraft parts.

The frequency of multipulses is the major factor for the localization of the delamination (Sezer and Li, 2009). At low frequency (around 1 Hz), the crack initiates at the BC/substrate interface due to several thermal shock cycling and the associated thermally grown oxide. At high frequency (around 10 Hz), it is located at the BC/TBC interface which is a major threat to the integrity of the engine. The integrity of the component is assessed by the delamination length: the larger, the more harmful. The delamination length increases with the angle beam and is commonly measured in the cross section of the hole (Sezer et al., 2006; Voisey et al., 2001; Kamalu et al., 2002) using optical micrographs.

Results in literature refer to a nickel-base superalloy substrate. The material drilled in this study is the cobalt-base superalloy (Haynes 188 (HS188 or ams5608)) which offers high strength and oxidation resistance to 1100 °C (Van Deventer, 1977) and is used in turbine engine typically working at 2000 °C. The substrate is covered with a ceramic coating. The present work aims at describing and quantifying delamination induced by percussion laser drilling at various angles on this multilayer material. Laser repetition rate is 10 Hz. Thus, the observed crack is expected to be located at the BC/TBC interface. The first section goes over longitudinal section observations of the holes pulse after pulse with a new approach to observe the evolution of the crack. The second section shows a new investigation to observe the morphology of the crack surface always with a micrography observation. Furthermore, visualization in real time of the laser drilling with a fast camera allowed us to discuss phenomena in relation with material observations.

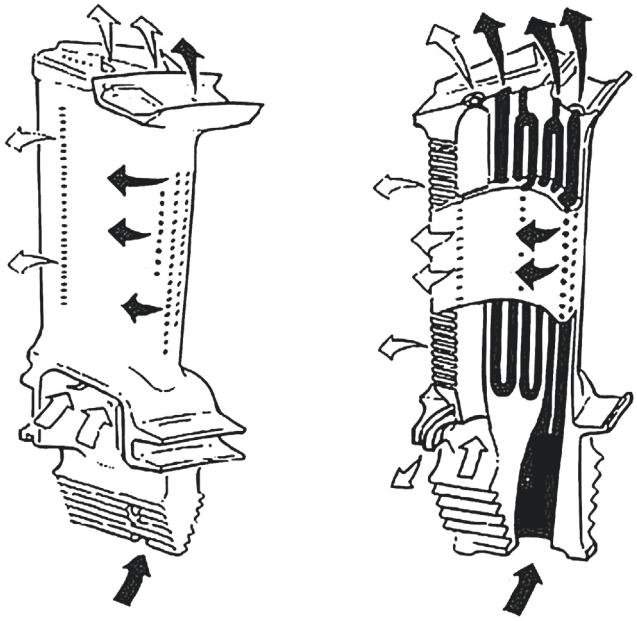

Fig. 2. Representation of the cooling method of turbine blade using thousands of holes in which a cool air is flowing in a turbine blade.

Table 1
Plasma spraying parameters.

Ceramic layer powder	YSZ
Binding layer powder	NiCrAlY
Ceramic layer plasma gas flow	30 l/min (Ar)
Binding layer plasma gas flow	4 l/min (H_2)
Spray distance	80 mm
Number of passes	from 5 to 10

2. Experimental set up

2.1. Materials

The laser-drilled material was a multilayer material. The metal substrate was a cobalt-base superalloy used in the manufacture of aircraft components. Its denomination is “Haynes 188” or “HS188” or “ams5608”. A nickel/chromium (NiCrAlY) bond coating was first sprayed on the workpiece surface to enhance the adhesion of the thermal barrier coating. The thickness of the BC is around 0.2 mm. The TBC consisted of a Zirconium–Yttrium oxide ceramic and is 0.5 mm thick. The manufacturing process is the conventional plasma spraying (Fauchais, 2004) and parameters are listed in Table 1. Laser drilling was carried out on sheets of 2 mm.

2.2. Process and fast camera parameters

The laser source is a TRUMPF HL201p (Nd:YAG) operating at 1.064 μm. It delivers a reliable circular and uniform spatial intensity distribution of light. The beam spot diameter can be fixed whatever the peak power of the laser source. It was here equal to 300 μm. The absorbed intensity which is the effective energy can be deduced from the peak power measurement (Schneider et al., 2007a, 2008). In this study, the incident intensity, so called I_{inc}, was held constant and equal to 18.4 MW/cm^2 which coresponds to a peak power of 13 kW. The focal distance was held constant for all the drillings. The work piece was drilled from TBC side. One to eight pulses with a frequency of 10 Hz were delivered. The pulse duration is 1 ms. The shot angles, so called β, were selected equal to 20°, 30° and 40° because they induced delamination on nickel-base superalloy AM1 with coating (Kamalu et al., 2002). Shots at 90° were also performed as shot references. Oxygen assist gas was used coaxially with the laser beam via a 1.5 mm exit diameter converging nozzle. The gas pressure was held constant at 6 bar.

The laser process parameters are listed in Table 2:

A Photron RS 250k camera with a band pass filter was used to investigate the fluid ejection dynamics following the work of Schneider et al. (2007a). The experimental set up is described in

Table 2
Laser process parameters.

Laser source	TRUMPF HL201p (Nd:YAG)
Laser incident intensity	I_{inc} = 18.4 MW/cm^2
Beam diameter	300 μm
Pulse duration	1 ms
Assist gas	O_2
Shot angle	β = 40°, 30° and 20°
Number of pulse	from 1 to 8 pulses
Repetition rate	10 Hz

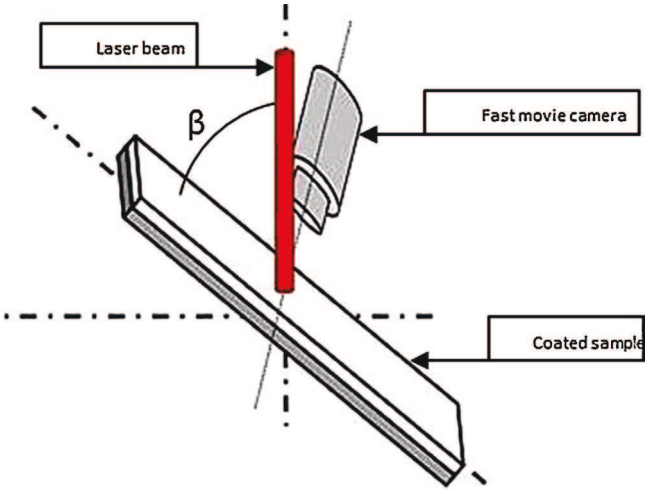

Fig. 3. Experimental set up for the fluid ejection visualization.

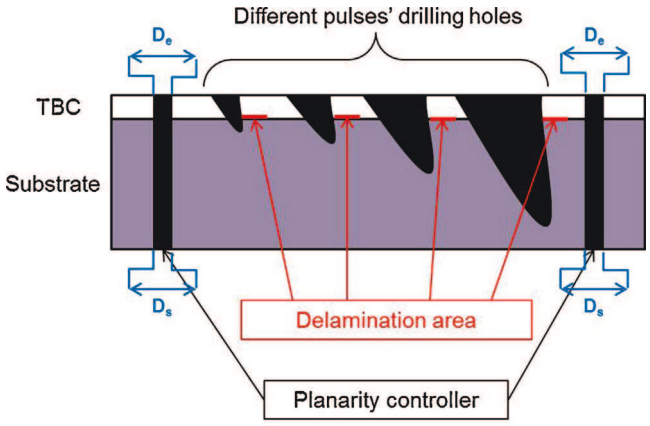

Fig. 4. Representation of the sample used for longitudinal section observations.

Fig. 3. The band pass filter is used because the lighting were chosen monochrome and provided by a laser diode. The shot frequency of the fast movie camera was 100,000 fps (1 frame for every 10 μs) with a resolution of 128 × 80 pixels. The trigger was synchronized with the laser beam.

2.3. Longitudinal section observation

The aim of longitudinal section observations is to investigate the delamination evolution laser pulse after laser pulse. Each sample contains one column of aligned four holes got for fixed absorbed intensity, time pulse, focal distance and shot angle equal to 20°, 30° or 40° but increasing number of laser pulses. Two holes drilled at 90° to the sample surface at the boundaries of the hole set are used as planarity gauge of the cross section (Fig. 4 shows four inclined holes and the two holes at 90°). Here, we focused on delamination. After drilling, the samples were sectioned at 2 mm from the edge of the holes. Then, they were cold-covered with polyamide. They were mechanically polished until the middle plane of the hole. In order to assess that the middle plane is reached for all the holes of one sample, the entrance and exit diameters (D_e and D_s) of holes drilled with normal angle of incidence were measured and checked to be equal. The polishing was ended by electrochemical etching for approximately 3 s using a mixture of phosphoric acid (H_3PO_4; 10%) and deionised water with 15 V DC. Longitudinal section were observed using optical microscopy.

2.4. Cross section observation

In order to characterize the geometry of delamination, drilled samples were observed in a parallel plan at the work piece surface. The observation plan is shown in Fig. 5 and is labeled as B–B view.

The sample preparation is similar to the preparation used for longitudinal section observations. After drilling, the sample was sectioned far from the region of interest. As for longitudinal section observation, they were cold-covered with polyamide but this time under vacuum. In addition, the polyamide was preliminary black colored. As a result, the polyamide soaked into the porosity made by the delamination revealing the crack in optical observations. A mechanical abrasive polishing is used to reach the wanted depth at the B–B view. Microscope specific light is absorbed by the TBC because of its high porosity. Tangential light was preferred to enhance optical observations. In such conditions, the ceramic is white and the crack is black because of the presence of the black polyamide.

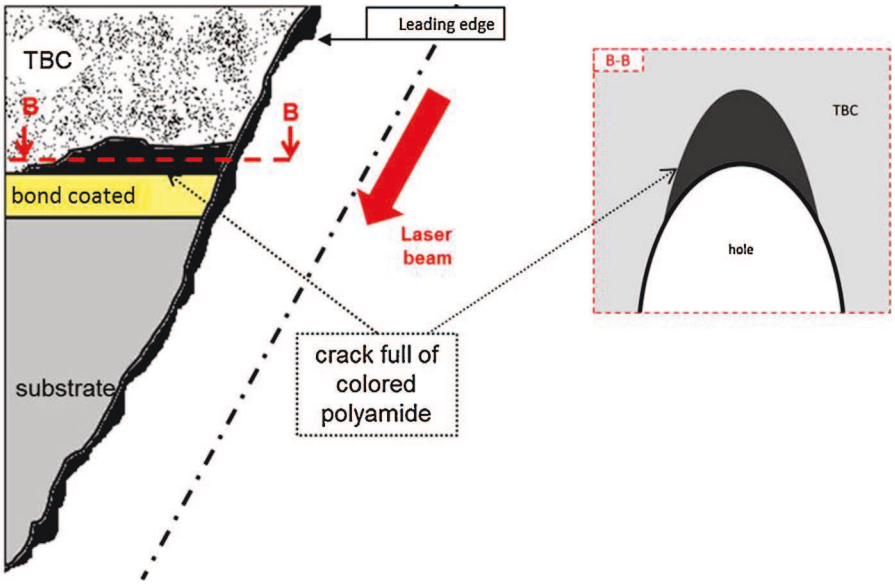

Fig. 5. Schematic representation of the delamination.

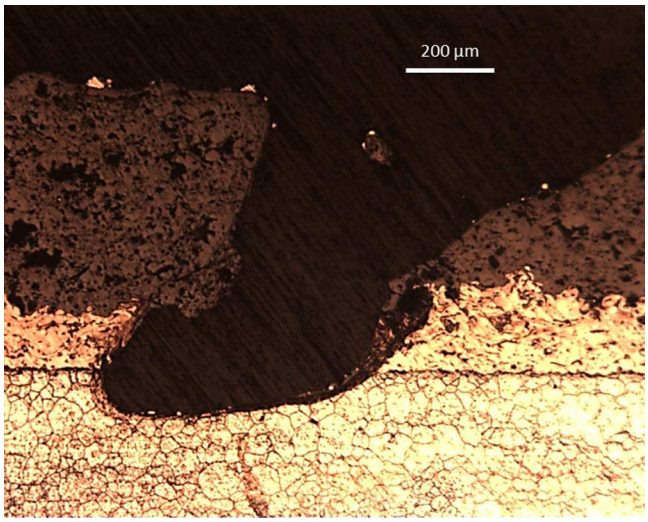

Fig. 6. Hole micrograph. (I_{inc} = 18.4 MW/cm^2; β = 40°; 1 pulse).

3. Results

3.1. Longitudinal section observation

Figs. 6–9 show longitudinal section micrographies of holes angles at 40° to the workpiece surface after one, two, three and four pulses:

- The first laser pulse (Fig. 6) produced a hole which only broke through the two coated layers. The hole penetrated less than 100 µm into the metallic substrate and no crack occurred.
- At the second laser pulse (Fig. 7), the hole penetrated at 1 mm into the substrate and several defects are observed. Firstly, the hole diameter in the ceramic coating is smaller than in the BC and metallic substrate. In other word, the hole profile changed as the interface is crossed. Moreover, a thick recast layer of a mixture of ceramic and metal is observed around the BC/substrate interface at both leading and trailing edges though it is thicker at the trailing side. A delamination crack is observed at the leading edge, in the TBC but very closed to the TBC/BC interface as expected from literature (Sezer and Li, 2009) and its length is 0.23 mm. As report in (Sezer et al., 2006), Fig. 7 shows also the different characteristics layers in laser drilling of metal, and especially the recast layer.
- At the third laser pulse (Fig. 8), the hole penetrated at almost 2 mm into the metallic substrate. The hole diameter slightly decreases with depth and is uneven. This is due to the presence of localized resolidified layer at the trailing edge. The delamination length increases and its value is 0.85 mm.
- The fourth laser pulse (Fig. 9) corresponds to the breakthrough of the coated sheet for a 40° shot angle. The melt is no more ejected upwards through the hole entrance but is flushed downward the hole exit. The delamination crack length does not increase anymore regarding to measurement errors.

Similar observations were found for laser drilling at 30° and 20°. Fig. 10 reports the delamination crack length with respect to the number of pulse for the three different drilling angles 40°, 30°, and 20°. Each value is the average of two measurements done on isoparameter samples. Despite these few numbers of samples, the tendency is in a good agreement with the literature results (Voisey et al., 2001; Kamalu et al., 2002). Standard deviation is represented

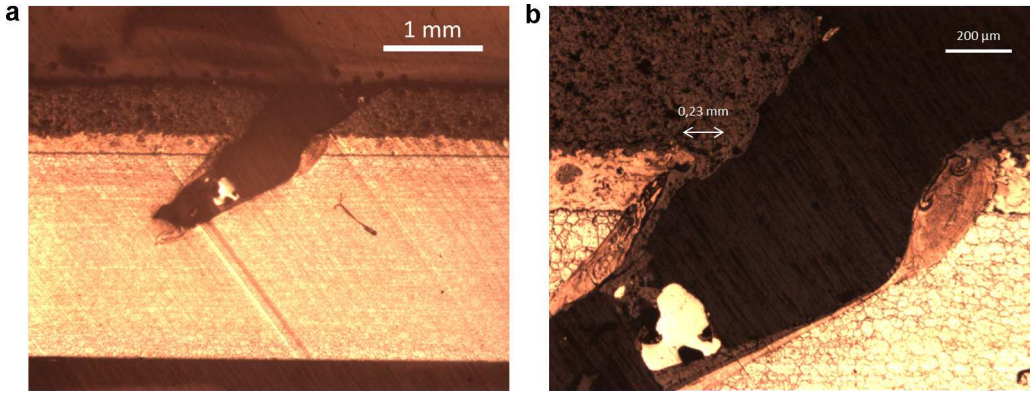

Fig. 7. Hole micrograph (a) and delamination zoom (b). (I_{inc} = 18.4 MW/cm^2; β = 40°; 2 pulses).

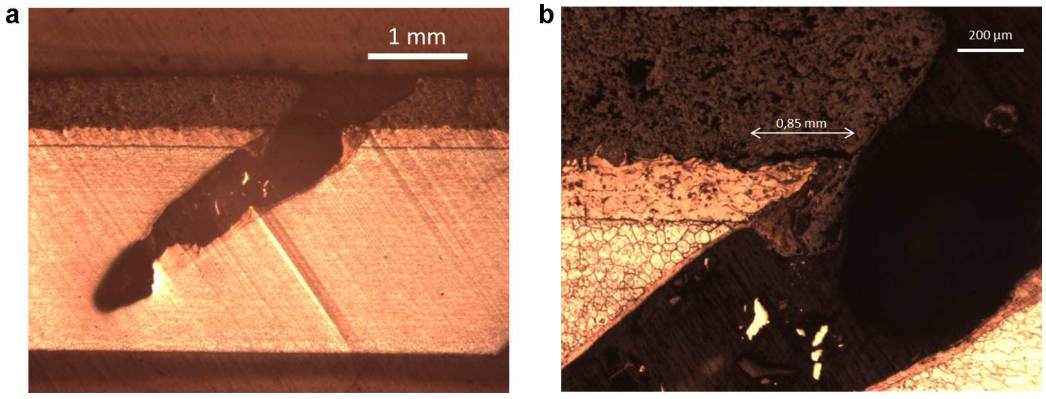

Fig. 8. Hole micrograph (a) and delamination zoom (b). (I_{inc} = 18.4 MW/cm^2; β = 40°; 3 pulses).

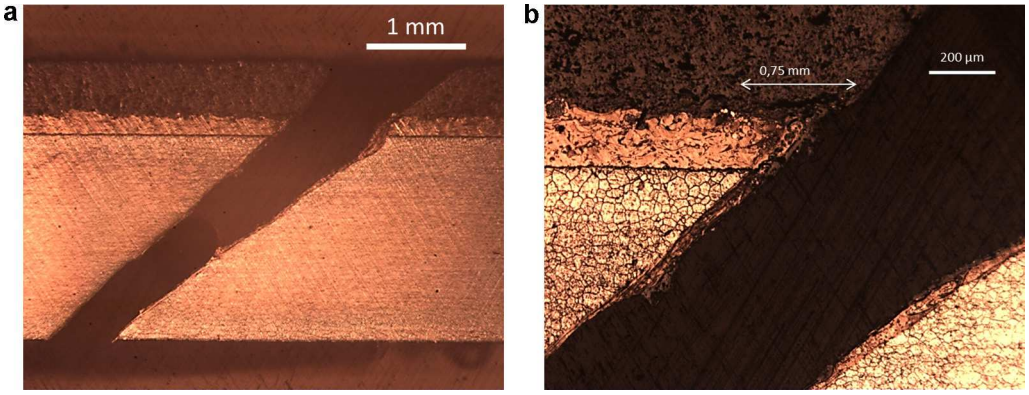

Fig. 9. Hole micrograph (a) and delamination zoom (b). (I_{inc} = 18.4 MW/cm^2; β = 40°; 4 pulses).

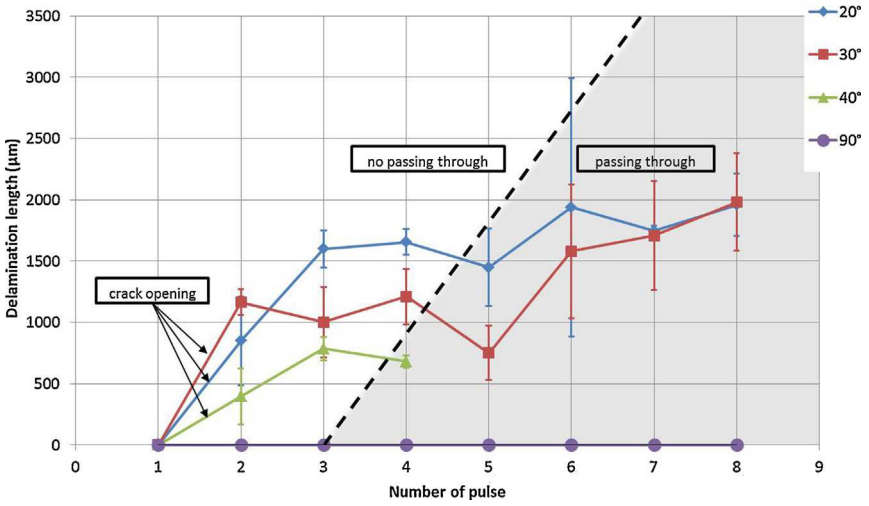

Fig. 10. Evolution of delamination length for three drilling angles (β = 40°, 30° and 20°).

by error bars. The delamination crack length increases with decreasing drilling angle to surface as found for coated nickel-base superalloys (Voisey et al., 2001; Kamalu et al., 2002). Indeed, for a 3 pulse hole, delamination length is equal to 0.7 mm with a 40° shot angle, 1 mm with 30° and 1.6 mm with 20°. At 90°, no delamination occurs as shown in Fig. 11. However, the shouldered shape of the hole at the TBC/substrate interface mentioned above is also observed. Measured lengths are consistent with results found in literature for a coated nickel-base superalloy substrate (Sezer and Li, 2009). Fig. 12 shows the crack area for a delamination crack length of 2.2 mm induced by eight laser pulses with 20° shot angle. The crack path is not planar because it probably follows the BC/TBC interface roughness. However, the non-smooth and non-planar crack path makes difficult precise measurement of the crack front in the cross section micrograph. According to the author's knowledge, this issue was never mentioned in literature despite this method is systematically used (Sezer and Li, 2009; Kamalu et al., 2002). It explains why the error in delamination crack length measurements increases with the crack length in Fig. 10.

Fig. 11. Hole micrography. (I_{inc} = 18.4 MW/cm^2; β = 90°; 4 pulses).

4. Cross section observation

Fig. 13 displays coated sheet longitudinal section observations (along the B–B view) at three depths in ceramic. The laser angle to the surface is 20° and the pulse number is six.

Fig. 13(a) and (b) corresponds to the so-called depth 1 and 2 and are above the delamination crack. The elliptic trace of the black hole

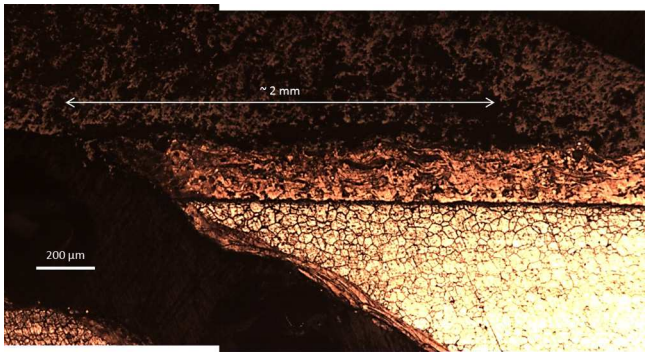

Fig. 12. Delamination zoom of the front crack area. (I_{inc} = 18.4 MW/cm^2; β = 20°; 8 pulses).

is marked using dashed line. The ceramic appears whitish and displays a very heterogeneous microstructure revealed by tangential light of the optical microscope. After the last polishing operation, the depth where the delamination crack is located was reached (Fig. 13(c)). The delamination crack corresponds to the dark zone (indicated by the red dashed line) got with soaked black polyamide (see Section 2.4). The 2D crack front is very winding but propagates mainly along the leading direction of the inclined hole. No crack was observed at other places. The delamination crack propagation is probably controlled by the ceramic porosity, the BC/TBC interface and the mechanical loading which takes place during the process. This point is discussed in the last section of the paper. The length of the crack in the 2D view is in good agreement with measurements obtained using cross section observations.

4.1. Fast camera movies

In order to understand why delamination occurs only at the second pulse, laser drilling operation in inclined angles of incidence were observed in real time with a fast camera. Results obtained for coated cobalt-base superalloy were compared to the literature results (Schneider et al., 2007b) obtained on the same metallic substrate but without coating to investigate the effect of the TBC in the laser process.

Fig. 14 shows fast camera images of the melt and gas ejection taken at the same time during the first pulse fired at 90° to the surface for both systems (Co-base superalloy with and without TBC). According to Schneider et al. (2011), the hydrodynamic behavior of the gas ejected is straight related to the surface temperature of the vapor front during the process. Thus, surface temperatures can be estimated and is more than 5000 K for an incident intensity of 25.4 MW/cm^2 which corresponds to a 18 kW peak power for the laser source. The local pressure at the same range of intensity is about 100 bar. On the movies, a shock wave was observed during the drilling for both systems. This shows that gas behaviors were both supersonic but the size of the shock wave was almost two

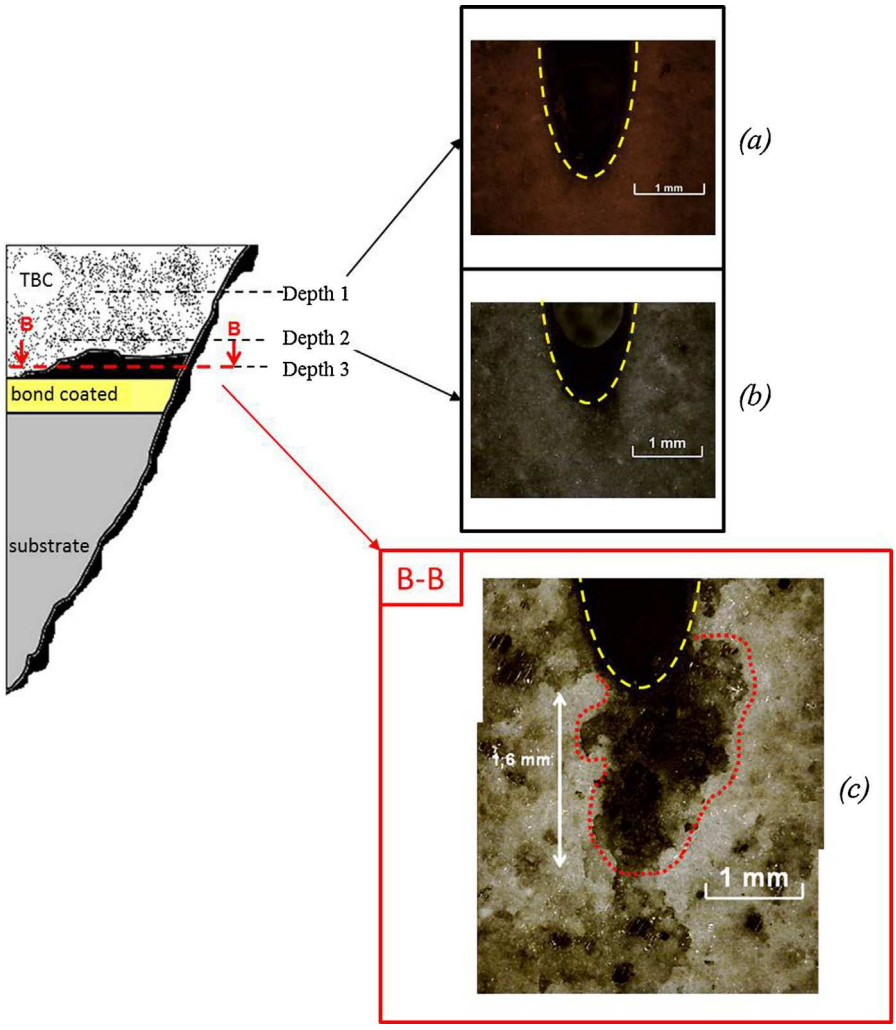

Fig. 13. Hole micrograph in the longitudinal section at three different depths (a), (b) and (c). (I_{inc} = 18.4 MW/cm^2; β = 20°; 6 pulses).

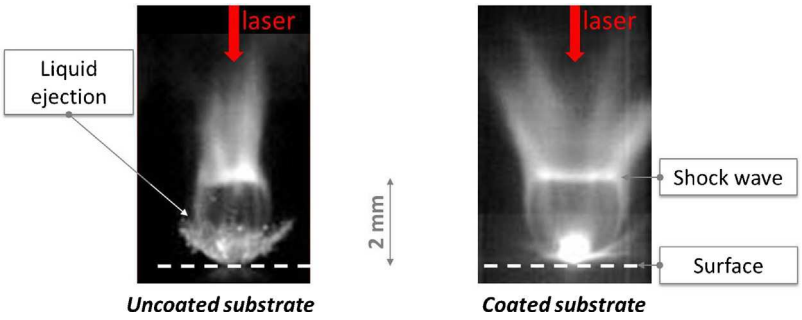

Fig. 14. Hydrodynamics of the gas ejection on the uncoated substrate (a) and the coated substrate (b) during laser drilling at normal angle of incidence. (I_{inc} = 25.4 MW/cm^2; β = 90°).

times larger in the case of coated substrate drilling than in the case of uncoated substrate drilling. This indicates that the temperature and ejection speed are much higher for a ceramic/laser than for a metal/laser interaction. Besides, for the drilling on uncoated substrate, liquid ejection as drops was observed on the edges of the ejection area for free-TBC substrate.

Since the first three pulses are responsible for the main part of the delamination crack length, the hydrodynamics of the vapor and melt were registered for drilling at 20° to the surface for the coated substrate. The incident intensity was also selected equal to 25.4 MW/cm^2. Fig. 15 shows the fluids ejection for the three pulses at 300 μs after the beginning of the pulse.

The fluid ejection for the first pulse is far different from the two others. This change corresponds to the instant at which the hole penetrates into the substrate and reveals the change between ceramic/laser and laser/metal interaction. During the first pulse associated with ceramic/laser interaction, the fluid ejected seems to be mainly gaseous whereas it is mainly liquid for the second and the third pulses associated with metal/laser interaction.

5. Discussion

Laser drilling at acute angles of coated superalloys in industry involves complex phenomena mainly related to the fact that the ceramic TBC and the metallic substrate have very different thermal and mechanical properties and also that the drilling at acute angles is a non-symmetrical process inducing different types of damage around the hole.

Fast camera analysis showed that the presence of TBC induces a much higher surface temperature when the hole penetrates into the substrate than in the substrate depth whatever the laser beam of incidence. The first consequence is a taper shape of the hole through the sheet thickness since the temperature surface decreases with increasing depth. The second consequence is a shouldered shape of the hole at the TBC/substrate interface. The thickness of the molten zone and removed material is higher in the substrate than in the ceramic due to the larger conductivity and the lower melting point of the superalloy. This result was previously suggested by Voisey and Clyne (2004) who predicted the thermal fields for a TBC/nickel-base superalloys (so similar to the TBC/cobalt-base superalloys studied here as far as thermal properties are concerned) using finite difference modeling. They showed the presence of a discontinuity in the thermal field at the TBC/substrate interface. The thickness of the molten zone is higher in the substrate than in the ceramic due to the larger conductivity and the lower melting point of the superalloy. The edge area of the smaller diameter hole in the ceramic act as stopper for the liquid ejection and can play a role in the delamination crack propagation as discussed later.

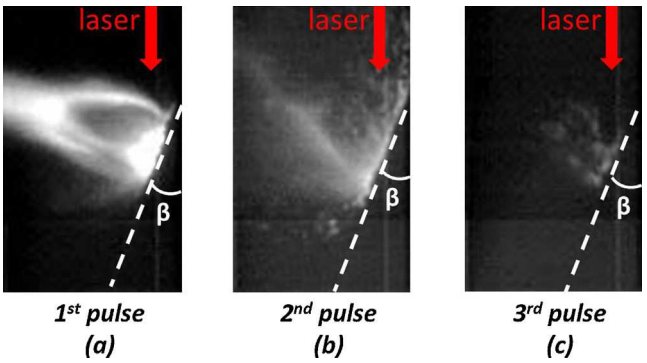

Fig. 15. Hydrodynamics of the gas and melt ejection on the coated substrate for the first pulse (a), for the second pulse (b) and for the third pulse (c). (I_{inc} = 25.4 MW/cm^2; β = 20°).

Investigations using cross optical micrographs revealed that at 90° laser beam incidence, no delamination crack was observed despite the presence of the shouldered shape of the hole.

Crack delamination appears at inclined drilling in the TBC at the BC/TBC interface at the leading edge but only from the second laser pulse when the laser beam interacts with the metallic substrate.

The crack is winding and not planar and propagates during the drilling process. Its propagation takes place along the BC/TBC interface and is directional from the hole leading edge. The overall propagation direction is contained in the middle cross plan of the hole. This shows that the delamination crack propagation path is mainly controlled by the TBC microstructure and mechanical stresses applying at the BC/TBC substrate. The crack propagation stops when the laser beam passes through the sheet sample.

Kamalu et al. (2002) assumed that initiation of delamination in thermal barrier coated nickel-base superalloy was related with steep thermal gradients produced when laser drilling. Thermally induced fracture between two pores in the TBC would be responsible for the delamination initiation. This mechanism should involve whatever the beam angle of incidence. However and on the contrary to Kamalu et al. (2002) results, no delamination was observed when 90° laser drilling. It is worth noticing that TBC/BC delamination was found below 0.2 mm for the normal incidence drilling, while it was consistently above 0.2 mm for the inclined holes in Kamalu et al. works. This maybe explains why the delamination was not observed at 90° drilling in this work. Sezer and Li (2009) suggested the key role of mechanical stresses induced by the upward melt ejection in the initiation and propagation of delamination without clearly distinguished the two stages.

As no significant delamination crack was observed at 90° laser drilling, we assumed that it was only due to mechanical stresses. Thermal effects are thus neglected. Fig. 16 illustrates two possible mechanical effects applying on the BC/TCB interface.

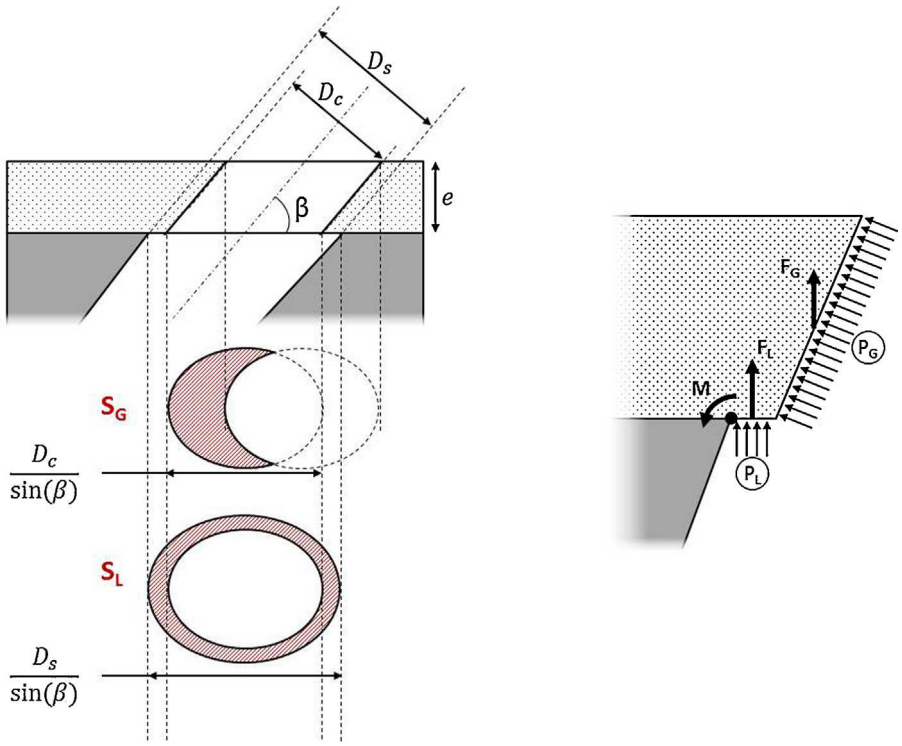

Fig. 16. Representation of the delamination model in inclined configuration.

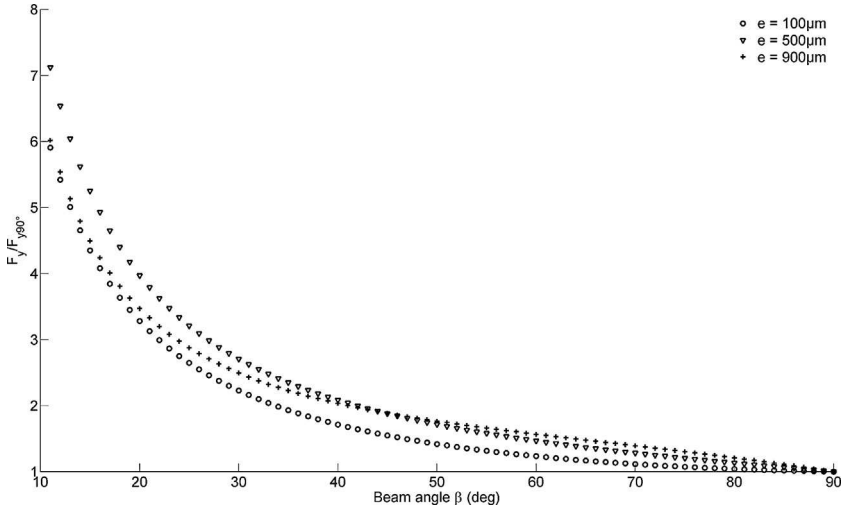

Fig. 17. Relative force F_y as a function of the beam angle of incidence for different TBC thickness.

As mentioned above, the ceramic at the hole shape discontinuity partially stops the melt ejection. As a result, the molten material applies a vertical force so called F_L (or equivalently the liquid pressure P_L) on the TBC as illustrated in Fig. 16. This effect takes place whatever the laser beam angle of incidence. Let us consider the hole diameters called D_c in the ceramic and D_s in the substrate. The angle beam is called β and e the TBC thickness.

The surface areas on which the liquid pressure P_L applied is S_L. According to Fig. 16, the surface S_L is calculated as a difference of two centered elliptic surfaces, due to the projection of two inclined cylinder following the vertical direction:

$$S_L = \left(\pi \frac{D_s}{2\sin(\beta)} \frac{D_s}{2}\right) - \left(\pi \frac{D_c}{2\sin(\beta)} \frac{D_c}{2}\right) = \frac{\pi}{4\sin(\beta)}(D_s^2 - D_c^2) \quad (1)$$

The liquid pressure can be calculated using the Bernoulli equation:

$$P_L = \frac{1}{2}\rho v_L^2 \quad (2)$$

ρ is the liquid density and is equal here to 6980 kg/m^3. The liquid velocity v_L was estimated using the fast camera analysis. Indeed, by comparing the position of a particle in the liquid flow at two different times, an average velocity was found about 50 m/s. As a result, P_L was estimated to 87 bar.

Besides, vapor pressure applies also on the inclined leading edge a vertical force so called F_G (Fig. 16). The surface area on which the gas pressure applies is S_G. S_G is calculated as the intersection of two shifted ellipses. The detail of the calculation is shown in Appendix

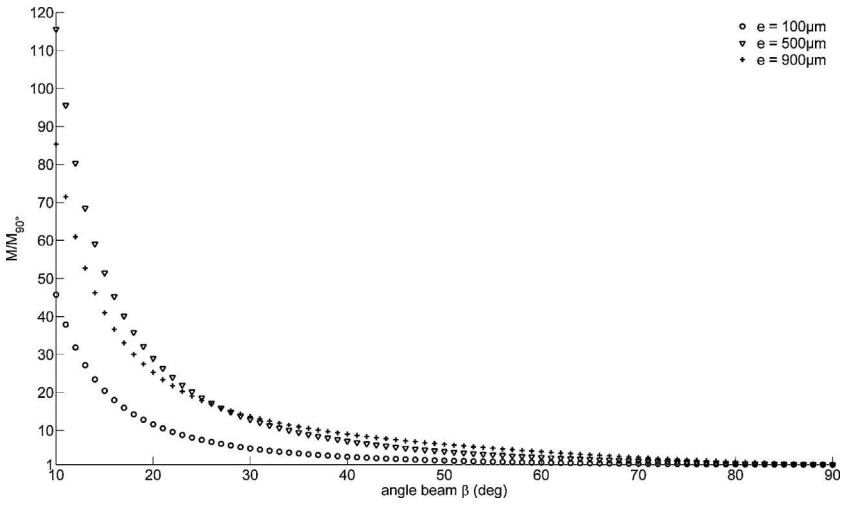

Fig. 18. Relative momentum M as a function of the beam angle of incidence for different TBC thickness.

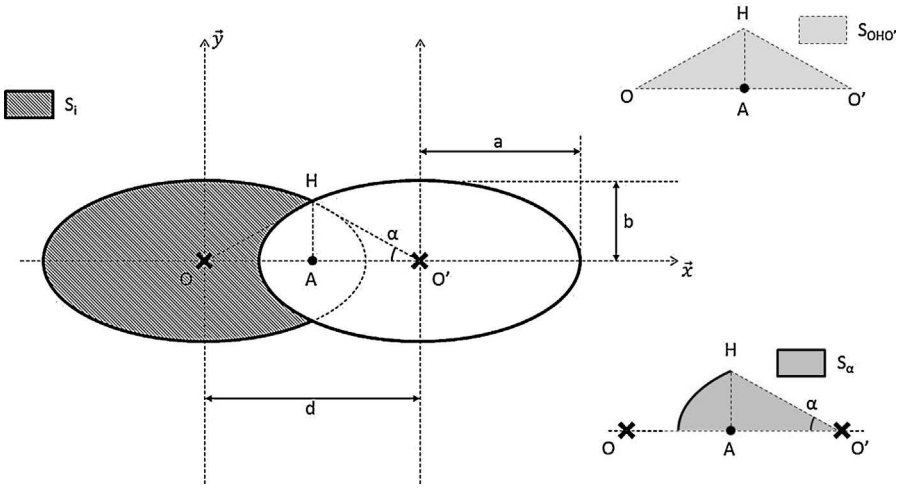

Fig. 19. Representation of the two ellipses and the surfaces S_i, $S_{OHO'}$ and S_α.

A. Thus, S_G is set with regards to the geometrical parameters:

$$S_G = \pi \frac{D_c^2}{4\sin(\beta)} - \frac{D_c^2}{2\sin(\beta)}\left(\alpha + \frac{\sin(2\alpha)}{2}\right) + \frac{eD_c}{2\tan(\beta)}\sqrt{\left(1 - \frac{e^2}{D_c^2}\frac{\sin(\beta)}{\tan^2(\beta)}\right)}$$

with

$$\alpha = \arctan\left(\frac{D_c}{e}\frac{\tan(\beta)}{\sin(\beta)}\sqrt{\left(1 - \frac{e^2}{D_c^2}\frac{\sin(\beta)}{\tan^2(\beta)}\right)}\right)$$

D_s and D_c are respectively equal to 700 µm and 500 µm.

The gas pressure P_G is specified in the works of Schneider et al. (2011). It comes from the Clapeyron equation and for the considered power density P_G is equal to 30 bar.

These two pressures, P_L and P_G, induce a resulting tensile vertical force and moment on the leading wall of the TBC/BC interface which favor crack propagation. The resulting force F_y can be written as the following sum:

$$F_y = F_L + F_G = P_L S_L + S_G \tag{4}$$

The momentum M due to the forces F_L and F_G on the point situated on the opening crack area (see Fig. 16) is calculated in the following way:

$$M = F_L\left(\frac{D_c - D_s}{4\sin(\beta)}\right) + F_G\left(\frac{D_c - D_s}{2\sin(\beta)} + \frac{e}{2\tan(\beta)}\right) \tag{5}$$

Note that Sezer and Li (2009) also introduced the possible damaging effect of the shear stress at the melt–wall interface due to the molten metal viscosity. We do not consider this effect in the following analysis.

Figs. 17 and 18 show the evolution of the force F_y divided by the same force at a beam angle of 90° and the momentum M due to F_y divided by the same momentum at a beam angle of 90°. Both values are plotted as a function of beam angle of incidence and are found much higher than 1 with beam angle lower than 90°. $F_y/F_{y90°}$ is equal to 4 for a 20° shot angle. $M/M_{90°}$ is equal to 40 for the same shot angle. These results demonstrate that mechanical effects can explain crack delamination and why the delamination crack length is larger for lower beam angle of incidence. They indicate that the gas pressure plays a dominant role mainly via a resulting momentum at the TBC/BC interface. Since the momentum depends on the TBC thickness, it suggests also that the TBC thickness should be

diminished to reduce the mechanical impact on crack delamination. Further experiments done with coated samples with different TBC thickness are needed to assess these theoretical results.

6. Conclusion

Interrupted laser drilling of TBC cobalt-base superalloy was carried out varying the beam angles of incidence. Crack delamination appears at inclined drilling in the TBC at the BC/TBC interface at the leading edge but only from the second laser pulse when the laser beam interacts with the metallic substrate. The laser drilling from the TBC side induces much higher temperature at the TBC/substrate interface than far from it. It results in the presence of a shoulder in the hole profile. This shoulder acts as stopper for the liquid ejection inducing tensile mechanical stresses at the BC/TBC interface and can favor delamination crack propagation. However, it was shown that the pressure due to both the molten metal and vapor applying on the inclined leading ceramic wall of the hole mainly responsible for crack delamination. It results in a vertical force and moment on the TBC/BC. Crack propagation is mainly controlled by mechanical stresses. However, it was shown that the crack path is governed by the microstructure of the ceramic and the roughness of the BC/TBC interface.

Acknowledgments

This work has been supported by an aeronautical industrial partner and the *National Research Agency* (ANR).

Appendix A.

The aim of this section is to calculate the surface called S_i with respect to the distance a, b and d by referring to Fig. 19.

A.1. Calculation of $S_{OHO'}$

The first step is to obtain the surface of the triangle described by the three points $\{O\,H\,O'\}$. The length of the segment $||AH||$ is deduced of the cartesian description for an ellipse with the semi-minor and semi-major axis a and b:

$$\frac{x^2}{a^2}+\frac{y^2}{b^2}=1 \tag{A1}$$

By taking $x = d/2$, the length $||AH||$ is:

$$\left\|AH\right\| = b\sqrt{\left(1-\frac{d^2}{4a^2}\right)} \tag{A2}$$

and the surface of the triangle $\{O\,H\,O'\}$, what we will call $S_{OHO'}$, is:

$$S_{OHO'} = \frac{db}{2}\sqrt{\left(1-\frac{d^2}{4a^2}\right)} \tag{A3}$$

A.2. Calculation of S_α

The second step is to obtain the surface of the circular sector described by the angle α. This surface will be called $(\widehat{O'HO})$. The angle α which corresponds to the S_α angle is obtained by trigonometry:

$$\alpha = \arctan\left(\frac{2b}{d}\sqrt{\left(1-\frac{d^2}{4a^2}\right)}\right) \tag{A4}$$

and as the circular sector surface S_θ for an anyone θ angle in an ellipse is:

$$ab\int_0^\theta \frac{1+\cos(2u)}{2}du \tag{A5}$$

the surface S_α is then:

$$S_\alpha = ab\left(\frac{\alpha}{2}+\frac{\sin(2\alpha)}{4}\right) \tag{A6}$$

A.3. Calculation of S_i

By a linear combination of these different surfaces, S_i is equal to

$$S_i = \pi ab - 2(2S_\alpha - S_{OHO'}) = \pi ab - 2ab\left(\alpha+\frac{\sin(2\alpha)}{2}\right) + db\sqrt{\left(1-\frac{d^2}{4a^2}\right)} \tag{A7}$$

References

Fauchais, P., 2004. Understanding plasma spraying. Journal of Physics D: Applied Physics 37, R88–R108.

Kamalu, J., Byrd, P., Pitman, A., 2002. Variable angle laser drilling of thermal barrier coated nimonic. Journal of Materials Processing Technology 122 355–362.

Schneider, M., Berthe, L., Fabbro, R., Muller, M., 2008. Measurement of laser absorptivity for operating parameters characteristic of laser drilling regime. Journal o Physics D: Applied Physics 41, 15502.

Schneider, M., Fabbro, R., Berthe, L., Muller, M., 2007a. Study of hole properties in percussion regime with a new analysis method. Journal of Laser Micro/Nanoengineering 2, 128–132.

Schneider, M., Fabbro, R., Berthe, L., Muller, M., 2007b. Influence of incident angle on laser drilling. In: Proceedings in ICALEO, pp. 641–646.

Schneider, M., Girardot, J., Berthe, L., 2011. Recoil pressure and surface temperature in laser drilling. In: Proceedings in ICALEO.

Semak, V.A.M., 1997. The role of recoil pressure in energy balance during laser materials processing. Journal of Physics D: Applied Physics 30 2541–2552.

Sezer, H.K., Li, L., 2009. Mechanisms of acute angle laser drilling induced thermal barrier coating delamination. Journal of Manufacturing Science and Engineering 131, 01014.

Sezer, H.K., Li, L., Schmidt, M., Pinkerton, A.J., Anderson, B., Williams, P., 2006. Effect of beam angle on HAZ, recast and oxide layer characteristics in laser drilling o TBC nickel superalloys. International Journal of Machine Tools and Manufacture 46, 1972–1982.

Van Deventer, E.H., 1977. Hydrogen permeability of Haynes alloy 188. Journal o Nuclear Materials 66, 325–328.

Voisey, K.T., Clyne, T.W., 2004. Laser drilling of cooling holes trough plasma sprayed thermal barrier coatings. Surface and Coatings Technology 176 296–306.

Voisey, K.T., Thompson, J.A., Clyne, T.W., 2001. Damage caused during laser drilling of thermal spray TBCs on superalloy substrates. In: Proceedings in ICALEO.

Voisey, K.T., Westley, J., Byrd, P., Clyne, T.W., 2004. Effects of assist gas in the laser drilling of thermal barrier coated superalloys. In: Proceedings in ICALEO.